Metrol. Meas. Syst., Vol. 31 (2024) No. 4, pp. 711–731
DOI: 10.24425/mms.2024.152053

PAN POLSKA AKADEMIA NAUK

METROLOGY AND MEASUREMENT SYSTEMS
Index 330930, ISSN 0860-8229
www.metrology.wat.edu.pl

M&MS

COMPUTATIONAL FLUID DYNAMIC AS AN ENGINEERING TOOL FOR THE RECONSTRUCTION OF BLOOD HEMODYNAMICS AND SPATIAL CONFIGURATION BEFORE AND AFTER ENDOLEAK APPEARANCE

Andrzej Polańczyk[1)], Aleksandra Piechota-Polańczyk[2)], Agnieszka W. Piastowska-Ciesielska[2)], Ihor Huk[3)], Christoph Neumayer[3)], Patricia Pia Wadowski[4)], Julia Balcer[5)], Michal Strzelecki[5)]

1) Faculty of Safety Engineering and Civil Protection, Fire University, ul. J. Słowackiego 52/54, 01-629 Warsaw, Poland (✉ *andrzej.polanczyk@gmail.com*)
2) Medical University of Lodz, Department of Cell Cultures and Genomic Analysis, ul. gen. L. Żeligowskiego 7/9, 90-752 Łódź, Poland
3) Department of Surgery, Division of Vascular Surgery, Medical University of Vienna, Währinger Gürtel 18-20, 1090 Vienna, Austria
4) Division of Angiology, Department of Internal Medicine II, Medical University of Vienna, Währinger Gürtel 18-20, 1090 Vienna, Austria
5) Institute of Electronics, Lodz University of Technology, Al. Politechniki 10, 93-590 Lodz, Poland

Abstract

Endovascular aneurysm repair (EVAR) has emerged as the primary treatment option for abdominal aortic aneurysm (AAA) surgeries. The intricate hemodynamics within the AAA region often leads to various complications in post-stent-graft placement, such as endoleaks. Thus, the objective of this study was to assess the risk of stent-graft migration attributable to the appearance of endoleaks, employing spatial configuration analysis and wall shear stress (WSS) assessment. AngioCT data from 20 patients aged 50–60 years, who had undergone stent-graft placement at the Medical University of Vienna, were utilized. Three-dimensional geometries were reconstructed using ANSYS software (ANSYS, Canonsburg, Pa, USA) for blood flow simulation. The blood flow was assumed to be incompressible and laminar. The stent-graft's area and height were scrutinized, alongside the formulation of a shape factor connecting the real stent-graft's volume with a virtually reconstructed cylinder. Prostheses with endoleaks exhibited an average WSS of 328.23 ± 107.63 Pa, while the average WSS within the endoleak area was 30.00 ± 9.57 Pa. In contrast, prostheses without endoleaks displayed a WSS of 367.90 ± 119.42 Pa. Computational Fluid Dynamics (CFD) algorithms facilitated the analysis of WSS values pre- and post-endoleak appearance, as well as within the endoleak region. Additionally, the proposed shape factor facilitated the spatial configuration of stent-grafts with and without endoleaks, incorporating the pushing forces.

Keywords: Endoleaks, aortic stent-graft, CT, endovascular aneurysm repair, abdominal aorta, aorta visualization, vascular imaging.

Article history: received April 8, 2024; revised July 12, 2024; accepted September 5, 2024; available online October 16, 2024.

1. Introduction

Endovascular aneurysm repair (EVAR) has become the primary treatment option for *abdominal aortic aneurysm* (AAA) surgeries [1, 2]. The risk of aneurysm occurrence increases with age, with a higher incidence in men than in women [3]. It is observed that approximately 50% of patients with ruptured aneurysms reach the hospital alive, yet around 50% do not survive repair [4]. The complexity of hemodynamics in the AAA region may indicate several complications in patients after stent-graft placement, such as endoleaks [5, 6]. Endoleaks are areas where blood flow appears outside the lumen of the stent-graft after the EVAR procedure [7, 8]. Depending on the time of occurrence, stent-graft endoleaks are categorized as early, late, or recurrent [9, 10].

Moreover, according to White *et al.*, endoleaks are classified into five types: Type I involves leakage between the stent and the aortic or iliac wall (1a – proximal leak, 1b – distal leak, 1c – exclusion zone formed by an iliac plug with aorto-uni-iliac devices, 1d – "gutter"-like leak following fenestrated EVAR or chimney/periscope techniques); Type II entails aneurysm sac filling via a branch vessel (for abdominal EVAR: Patency of the inferior mesenteric or lumbar artery); Type III denotes leakage at the junction of stent-graft segments (IIIa – hole or defect within the stent-graft, IIIb – leak between two modular components, IIIc – defective stent-graft material); Type IV involves leakage across the graft due to its porosity, and Type V encompasses an "endotension" leak where no evidence of a leak site can be found, yet the aneurysmal sac continues to expand [11].

Medical imaging is a commonly used method in the diagnostic process [12]. Different techniques are utilized for detecting endoleaks, including angiography, conventional x-ray imaging, and computed tomography [13–15]. However, the most expedient and accurate method to confirm such a diagnosis is CT scanning of the AAA [16, 17].

Numerous studies have been published on the detection of apnoea events using individual signals recorded during polysomnography [18]. In recent years, the biomedical field has increasingly focused on developing continuous, non-invasive devices for monitoring blood pressure [19]. Also, plenty of studies have been conducted to explore new methods for blood pressure acquisition, including advancements in sensing materials, signal processing, and demodulation models [20, 21]. Moreover, different techniques are applied in healthcare to assess blood flow, and plethysmography is among the most accurate methods for detecting changes in blood volume within limbs, organs, and tissues [22]. While among *in vitro* methods, *particle imaging velocimetry* (PIV) is used to track the movement of reflective Particles within a flow channel [23]. Moreover, the *computational fluid dynamics* (CFD) technique may be employed for blood flow reconstruction [24, 25]. Additionally, the deep learning technique can be adopted for reconstructing blood vessel lumens [26].

Many studies have focused on the application of the CFD technique for blood flow reconstruction in the area of implanted stent-grafts [27, 28]. However, there is a lack of information directed towards CFD reconstruction of blood hemodynamics in the area of endoleaks. Therefore, the aim of this study was to describe the risk of stent-graft migration due to endoleak appearance by analysing its spatial configuration connected with wall shear stress analysis.

The manuscript is organized as follows: in Section 2, Material and Methods, medical data and the mathematical model with boundary conditions are described; in Section 3, Results, simulation results are presented; in Section 4, Discussion, the presented results are discussed.

2. Material and methods

AngioCT data (GE Light-Speed 64 VCT; GE Healthcare, Fairfield, CT, USA) from 20 Patients aged 50–60 years, who had undergone stent-graft placement for AAA at the Medical University of Vienna, were utilized. Medical data were retrospectively collected after obtaining written informed

consent to participate in the study and were anonymized before analysis. The study received approval from the local Institutional Review Board (2069/2012) of the Medical University of Vienna. All patients received the Zenith stent-graft manufactured by COOK (Cook Medical, USA) (Table 1, and contrast (Visipaque, GE Healthcare) was administered for radiological diagnosis (1.5 ml per 1 kg of body weight). Moreover, patient qualification for the study was based on the presence of a Type II endoleak observed in the upper Part of the prosthesis.

Table 1. Results of numerical experiments for stationary and nonstationary filters.

Patients	Main body diameter [mm]	Iliac leg diameter Left/Right [mm]
P1	28	10/12
P2	30	12/14
P3	28	12/12
P4	28	10/12
P5	30	12/14
P6	28	12/14
P7	28	12/12
P8	30	12/14
P9	30	12/12
P10	30	12/14
P11	28	12/12
P12	28	10/12
P13	30	14/14
P14	28	12/14
P15	30	12/12
P16	30	12/14
P17	30	12/12
P18	28	10/12
P19	28	12/12
P20	28	10/12

In the initial stage, *Digital Imaging and Communications in Medicine* (DICOM) data were utilized to create patient-specific 3D computer models of the endovascular prostheses placed in the AAA reconstruction, as previously described [29]. Anonymized AngioCT data ($512 \times 512 \times 270$ voxels, with an in-plane resolution of 0.78×0.78 mm and a slice thickness of 1 mm) from patients with Type II endoleaks formed the basis for this study. Digital segmentation involved manually adjusting brightness to achieve the highest contrast between the aorta and surrounding tissue, extracting the aorta from the background, and manually eliminating gaps using ImageJ software and its tool for morphological hole filling [30]. The implemented segmentation yielded accurate results; when compared to manual segmentation performed by a radiologist, the estimated aortas did not differ by more than 5%. Finally, after each segmentation process to reconstruct the 3D model of the aorta, rendering was performed [31].

Blood flow reconstruction was conducted using three-dimensional geometries and ANSYS software (ANSYS, Canonsburg, Pa, USA) [32]. Two groups were analysed: 20 geometries representing the spatial configuration of stent-grafts with endoleaks and 20 geometries representing the spatial configuration of stent-grafts without endoleaks (Fig. 1).

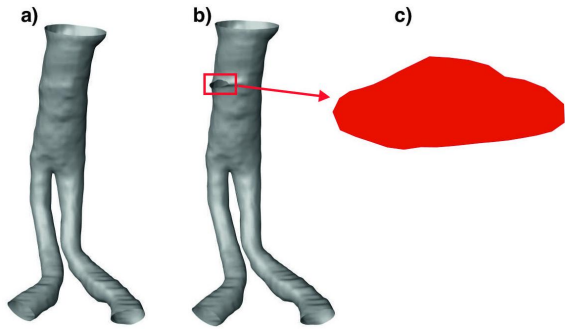

Fig. 1. Three-dimensional geometries: a) an example of stent-graft without an endoleak; b) an example of stent-graft with an endoleak; c) an example of an endoleak.

With the utilization of the ANSYS ICEM CFD pre-processor (ANSYS, Canonsburg, PA, USA), meshes consisting of 400,000 to 600,000 tetrahedral elements (achieved through mesh independence tests) were prepared. The Euler method was employed for solving the Navier–Stokes equations. Blood flow was assumed to be incompressible and laminar [33]. Velocity inlet $[v(x, y, z)]$, p = const at the outlets from the geometry and rigid wall (fluid-solid interface; the boundary condition $v = 0$ was utilized) were considered as boundary conditions [34]. The rheological properties of blood were characterized using Quemada's model (1 and 2) as previously described. The haematocrit (Hct) for all analysed patients was around 40% [35].

$$\eta = \eta_p \frac{1}{(1 - 0.5(K\mathrm{Htc}))^2}, \tag{1}$$

where: η_p – plasma viscosity, [Pa s]; K – inner viscosity of erythrocyte (2), [–]; Htc – hematocrit, [–].

$$K = \frac{\left(k_0 + k_\infty\left(\frac{\gamma}{\gamma_c}\right)\right)}{1 + 0.5\left(\frac{\gamma}{\gamma_c}\right)} \tag{2}$$

where: k_0, k_∞ – parameters which describes blood character, [–]; γ – shear rate value, [s^{-1}]; γ_c – critical shear rate value, [s^{-1}].

Therefore, in the CFD model, the Hct value was set at 40%. The blood velocity profiles for each of the analysed patients were obtained from USG-Doppler examination (GE Vivid 7, GE Healthcare, USA).

During blood flow, pushing forces characterized by *wall shear stress* (WSS) are present. Therefore, the mechanical aspect concerning WSS was included in the shape factor. Firstly, WSS was calculated (3).

$$\mathrm{WSS} = \int F \mathrm{d}A, \tag{3}$$

where: WSS – shear stress on the stent-graft's wall, [Pa]; F – force acting on a side surface of a stent-graft, [N]; A – side surface of a stent-graft, [m^2].

Next, the total value of WSS, characterizing one cardiac cycle (4).

$$\mathrm{WSS}_{\mathrm{tot}} = \sum_{k=1}^{n} \frac{\mathrm{WSS}(\Delta t_k)}{n} = \frac{1}{n} \sum_{k=1}^{n} \mathrm{WSS}(\Delta t_k), \tag{4}$$

where: $\mathrm{WSS}_{\mathrm{tot}}$ – total shear stress on the stent-graft's wall, [Pa]; $\Delta t_k = \Delta t$ for all k, [s]; n – number of time steps, [–].

For each patient, an operation of virtual erasing of the endoleak was performed. This allowed analysis of wall shear stress impact and prosthesis migration risk. The spatial configuration of 3D models was characterized by the use of the shape factor, previously described.

For the calculation of real volume, the stent-graft was treated as a cylinder (6), calculated from stent-graft's side surface (5).

$$\mathrm{AR} = \pi d h \rightarrow d = \frac{\mathrm{AR}}{\pi d}, \tag{5}$$

where: AR – real side surface of a stent-graft, [m^2]; d – diameter of a reference cylinder, [m]; h – height of reference cylinder and analysed stent-graft, [m].

$$V_r = 0.25(\pi \mathrm{d}^2) \rightarrow V_r = \frac{\mathrm{AR}^2}{\pi h} \tag{6}$$

where: V_r – volume of reference cylinder, [m^3]; d – diameter of reference cylinder, [m]; h – height of a reference surface and the analysed stent-graft, [m]; AR – real side surface of a stent-graft, [m^2].

The shape factor for the stent-graft with an endoleak was calculated as a relation of the real volume (V_r) of the stent-graft and virtually calculated (V_v) (7).

$$\mathrm{SWL} = \frac{V_r}{V_v}, \tag{7}$$

where: V_r – real volume of a stent-graft, [m^3]; V_v – virtually calculated volume of a stent-graft, [m^3].

Shape factor for the stent-graft without an endoleak was calculated as a relation of the real volume (V_r) of a stent-graft and virtually calculated (V_v) (8).

$$\mathrm{SWOL} = \frac{V_r}{V_v}, \tag{8}$$

where: V_r – real volume of a stent-graft, [m^3]; V_v – virtually calculated volume of a stent-graft, [m^3].

3. Results

3.1. Side surface of the prosthesis

Firstly, the influence of the prosthesis size on the WSS value was analysed. It was observed that prostheses with endoleaks are characterized by an average WSS equal to 63.28 ± 15.96 Pa. Additionally, the average WSS observed in the area of an endoleak was equal to 5.81 ± 1.62 Pa. In contrast, prostheses without endoleaks were characterized by an approximately 11% increase in the WSS value (70.95 ± 17.82 Pa) compared to the cases with endoleaks. Moreover, the analysis of prostheses with and without endoleaks indicated an increase in the WSS value with an increase in the prosthesis area. However, exceptions were observed: for prostheses with endoleaks (Fig. 2), the lowest WSS value (38.64 Pa) corresponded to an area of 0.021 m^2, while the highest WSS value

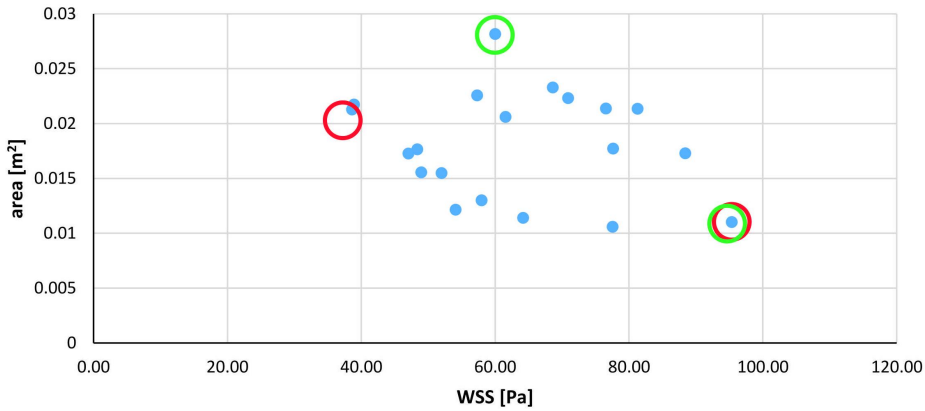

Fig. 2. Wall shear stress as a function of the prosthesis area with an endoleak. Wall shear stress was measured in [Pa] and prosthesis area was measured in [m^2]. Red circles indicate exceptional points for WSS values and green circles indicate exceptional points for area values.

(95.36 Pa) corresponded to an area of 0.01;m^2. Conversely, for the lowest area value (0.011 m^2), the WSS was 95.36 Pa, while for the highest area value (0.028 m^2), the WSS was 60.02Ṗa. The median was 60.80 Pa for an area of 0.018 m^2. Furthermore, for prostheses without endoleaks (Fig. 3), the lowest WSS value (42.76 Pa) corresponded to an area of 0.023 m^2, while the highest WSS value (104.79 Pa) corresponded to an area of 0.012 m^2. Conversely, for the lowest area value (0.012 m^2), the WSS was 435.65 Pa and 698.60 Pa, while for the highest area value (0.031 m^2), the WSS was 67.44 Pa. The median was 68.31 Pa for an area of 0.020 m^2. Moreover, the analysis for endoleaks (Fig. 4) indicated that the lowest WSS value (3.09 Pa) corresponded to an area of 0.0019 m^2, while the highest WSS value (8.54 Pa) corresponded to an area of 0.0010 m^2. Conversely, for the lowest area value (0.0010 m^2), the WSS was 4.06 Pa and 7.63 Pa, while for the highest area value (0.0028 m^2), the WSS was 6.30 Pa. The median was 6.24 Pa for an area of 0.0018 m^2.

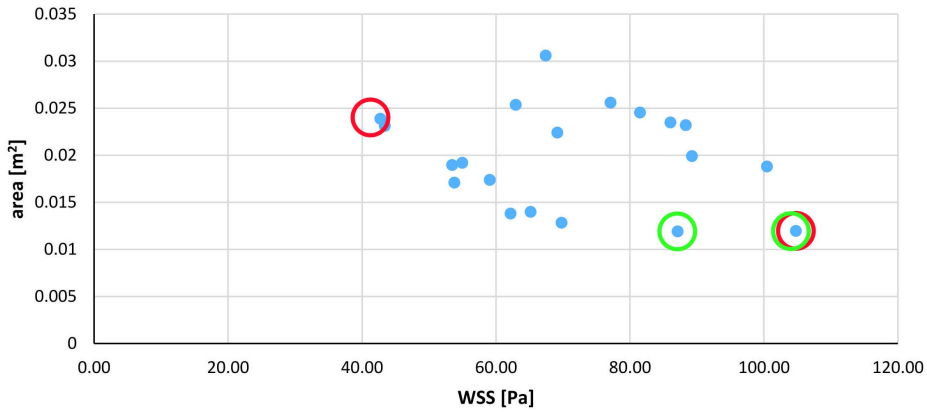

Fig. 3. Wall shear stress as a function of the prosthesis area without an endoleak. Wall shear stress was measured in [Pa] and prosthesis area was measured in [m^2]. Red circles indicate exceptional points for WSS values and green circles indicate exceptional points for area values.

Metrol. Meas. Syst., Vol. 31 (2024), No. 4, pp. 711–731
DOI: 10.24425/mms.2024.152053

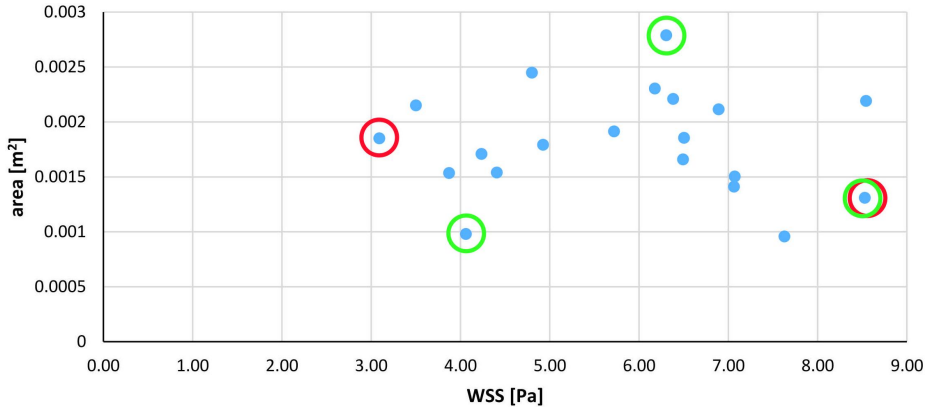

Fig. 4. Wall shear stress as a function of endoleak area. Wall shear stress was measured in [Pa] and endoleak area was measured in [m^2]. Red circles indicate exceptional points for WSS values and green circles indicate exceptional points for area values.

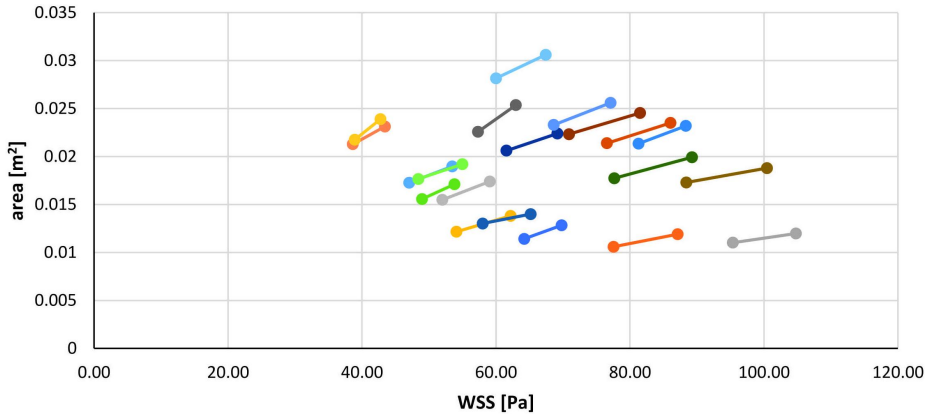

Fig. 5. Shift vectors for WSS values between prostheses with and without endoleaks. Wall shear stress was measured in [Pa] and prosthesis area was measured in [m^2].

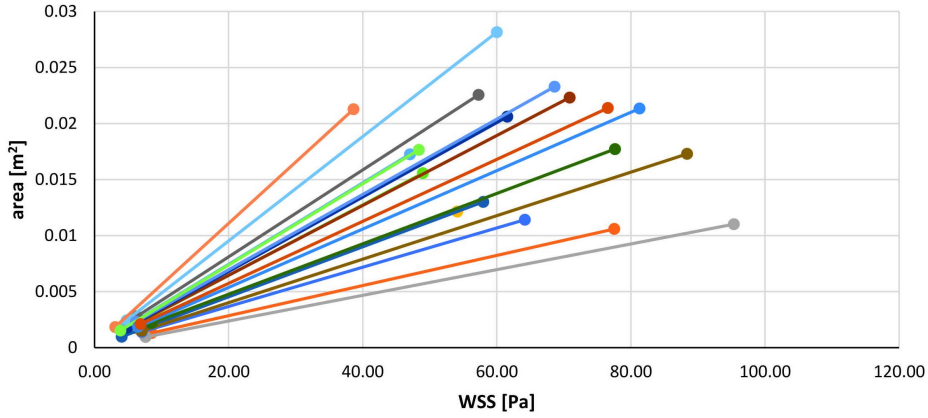

Fig. 6. Shift vectors for WSS values between prostheses with an endoleak compared to the endoleak area. Wall shear stress was measured in [Pa] and prosthesis and endoleak area were measured in [m^2].

Additionally, a shift vector (7.67 ± 2.26 Pa) was observed for WSS values between prostheses with and without endoleaks (Fig. 5). The highest shift was equal to 12.06 Pa, while the lowest was equal to 3.85 Pa. Furthermore, a comparison of prostheses with endoleaks to the endoleak area indicated that the highest difference was equal to 87.73 Pa, while the lowest value was equal to 35.41 Pa (Fig. 6).

A comparison of stent-grafts with and without endoleaks indicated an increase in the WSS value on the side surface of the prosthesis in the area of the endoleak (18.21 ± 0.4;Pa and 31.35 ± 0.52 Pa for stent-grafts without and with endoleaks, respectively) (Fig. 7 and Fig. 8). With an increase in the blood pressure value, higher pushing forces (WSS value) were observed in the lower Part of the prosthesis (54.61 ± 2.09 Pa and 42.38 ± 1.23 Pa for stent-grafts without and with endoleaks, respectively). However, for the prosthesis with endoleaks, an increase in the WSS value was also observed in the area of the endoleak (26.73 ± 1.0 Pa) (Fig 9). Moreover, it was observed that each time there occurred a lower WSS value than in the area of angulation in the lower Part of the prosthesis, it corresponded to lower WSS values (71.13 ± 3.11 Pa and 49.77 ± 2.86 Pa for

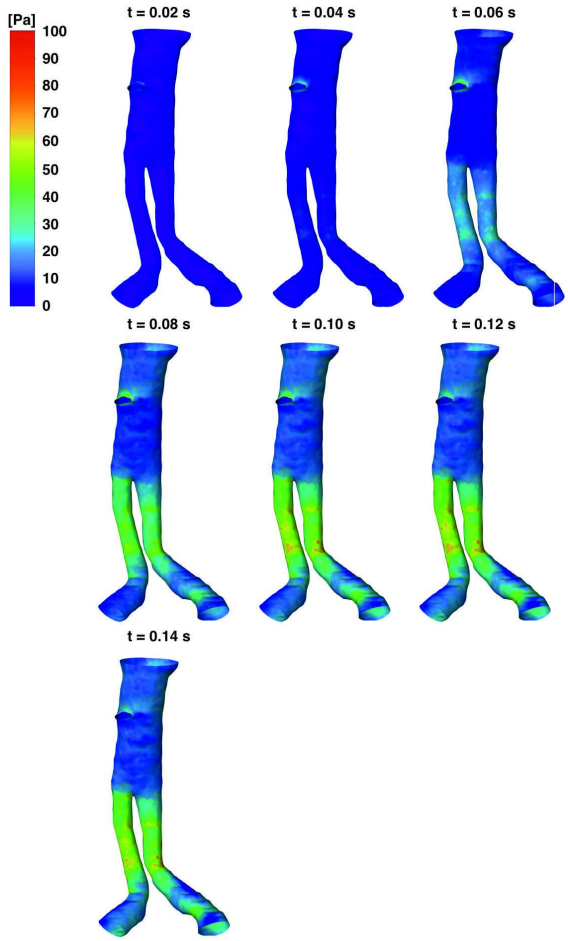

Fig. 7. Wall shear stress distribution for the representative stent-graft without an endoleak for different timesteps (0.02 s; 0.04 s; 0.06 s; 0.08 s; 0.10 s; 0.12 s; 0.14 s). Wall shear stress was measured in [Pa].

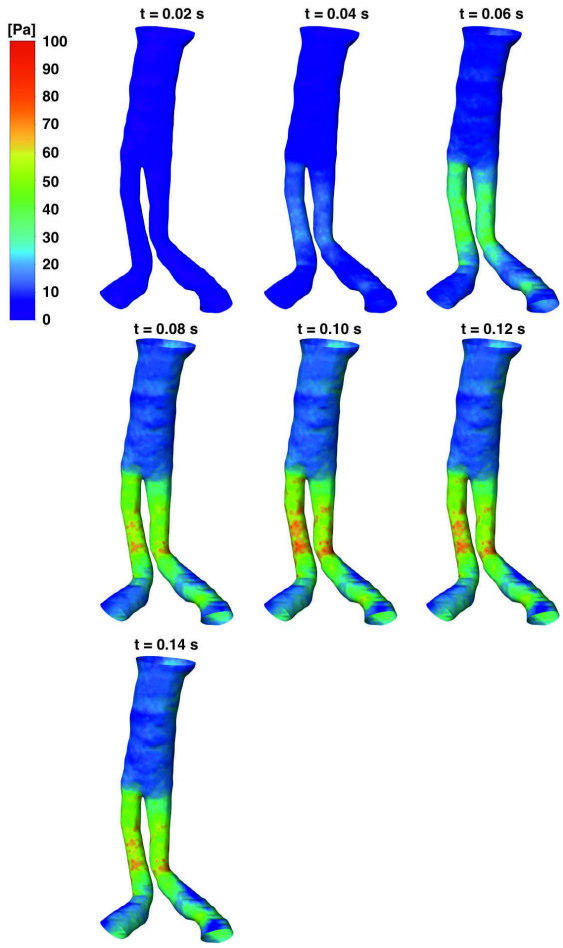

Fig. 8. Wall shear stress distribution for the representative stent-graft with an endoleak for different timesteps (0.02 s; 0.04 s; 0.06 s; 0.08 s; 0.10 s; 0.12 s; 0.14 s). Wall shear stress was measured in [Pa].

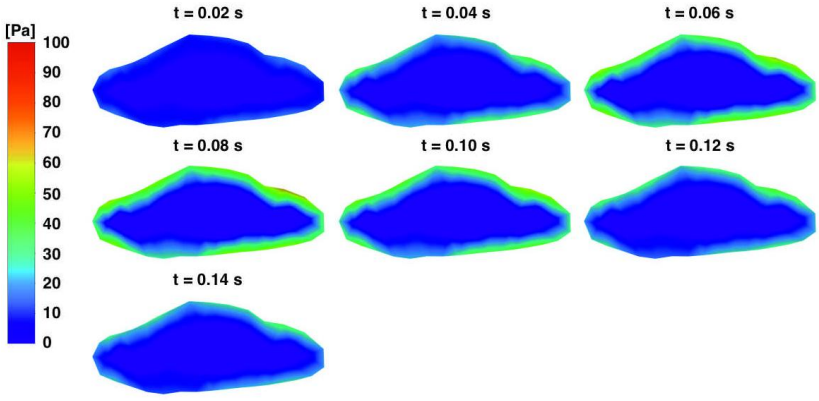

Fig. 9. Wall shear stress distribution for a representative endoleak for different timesteps (0.02 s; 0.04 s; 0.06 s; 0.08 s; 0.10 s; 0.12 s; 0.14 s). Wall shear stress was measured in [Pa].

stent-grafts without and with endoleaks, respectively). Our previous observations have indicated that this phenomenon contributes to a lower probability of prosthesis movement or even thrombus formation [36].

Moreover, a simultaneous decrease in WSS inside the stent-graft in the area of bifurcation was observed (Fig. 10 and Fig. 11). Furthermore, unequal distribution of WSS in the area of bifurcation was noted (41.04 ± 1.95 Pa (one leg) and 36.11 ± 1.01 Pa (the other leg) for stent-grafts without endoleaks, while 29.81 ± 1.63 Pa (one leg) and 22.45 ± 1.8 Pa (the other leg) for stent-grafts with endoleaks). Higher WSS values were consistently observed just below the bifurcation area (47.21 ± 2.21 Pa (one leg) and 42.33 ± 1.99 Pa (the other leg) for stent-grafts without endoleaks, and 35.21 ± 2.01 Pa (one leg) and 29.77 ± 1.77 Pa (the other leg) for stent-grafts with endoleaks). Moreover, the unequal distribution of WSS values was higher for prostheses without endoleaks compared to prostheses with endoleaks.

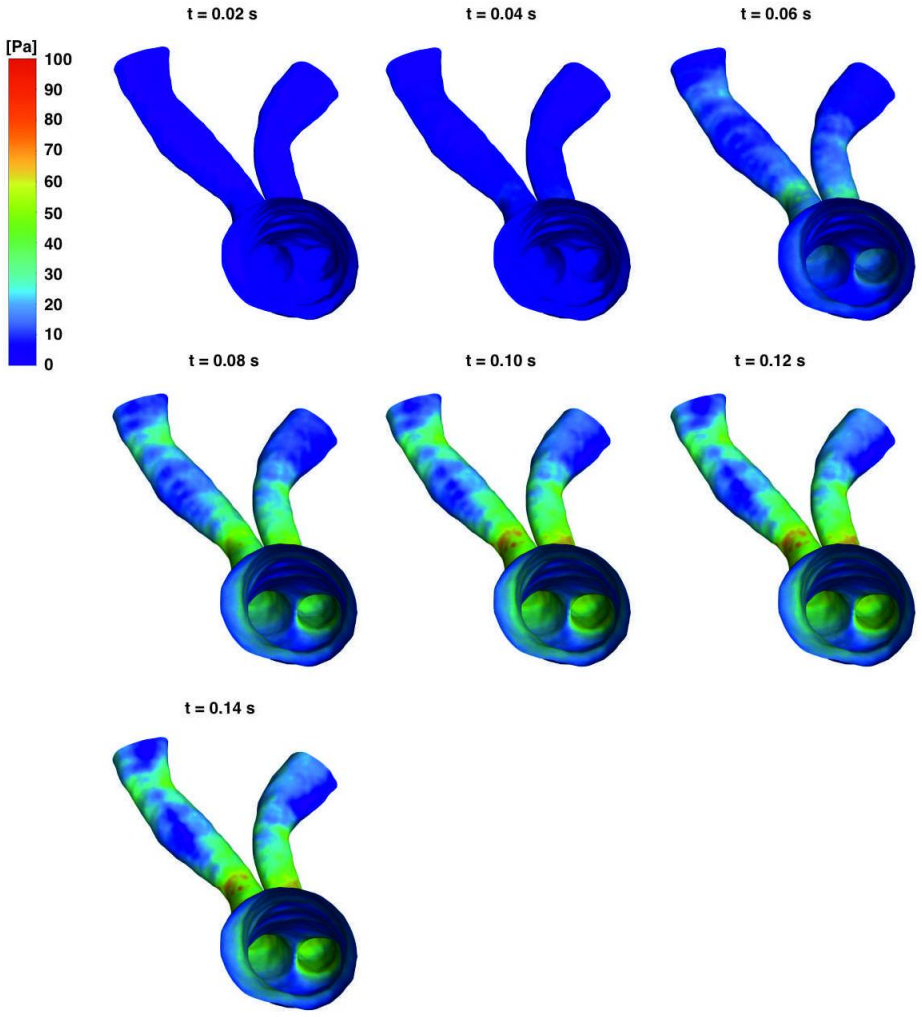

Fig. 10. Wall shear stress distribution in the area of bifurcation (interior view) for the representative stent-graft without an endoleak for different timesteps (0.02 s; 0.04 s; 0.06 s; 0.08 s; 0.10 s; 0.12 s; 0.14 s). Wall shear stress was measured in [Pa].

Metrol. Meas. Syst., Vol. 31 (2024), No. 4, pp. 711–731
DOI: 10.24425/mms.2024.152053

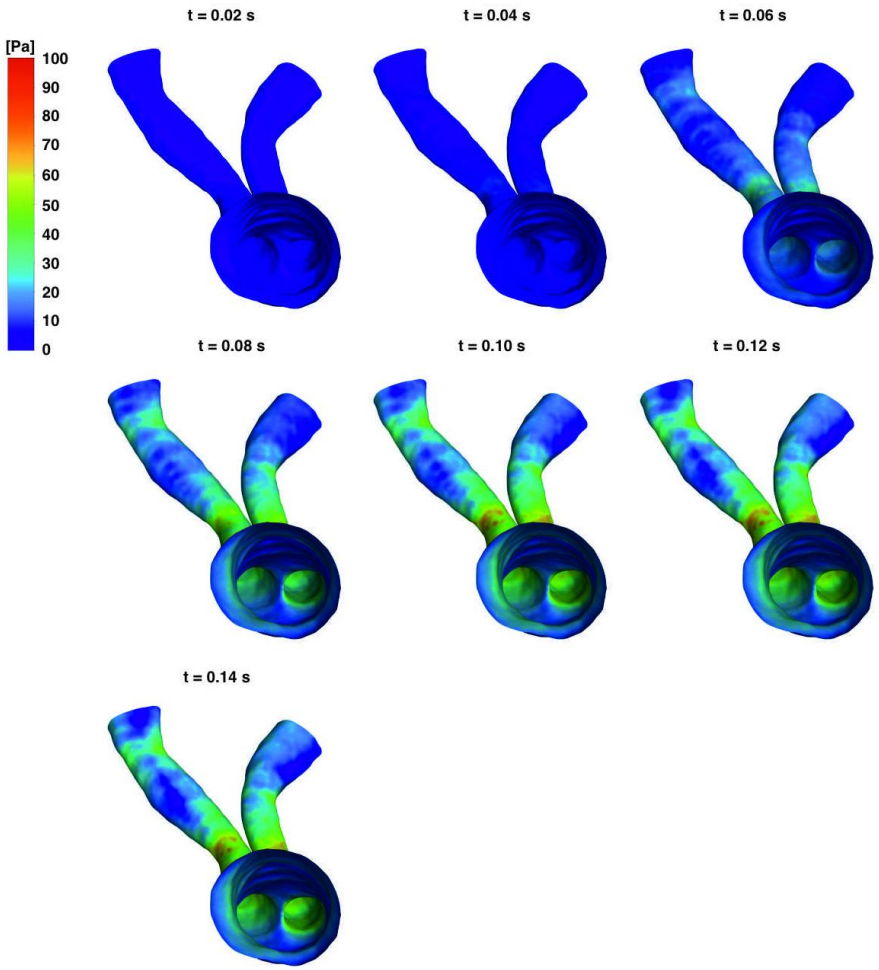

Fig. 11. Wall shear stress distribution in the area of bifurcation (interior view) for the representative stent-graft with an endoleak for different timesteps (0.02 s; 0.04 s; 0.06 s; 0.08 s; 0.10 s; 0.12 s; 0.14 s). Wall shear stress was measured in [Pa].

3.2. Height of the prosthesis

Next, the influence of the prosthesis height on the WSS value was analysed. Similar to the area analysis, it was observed that with an increase in prosthesis height, there was an increased WSS value. However, exceptions were observed: for prostheses with endoleaks (Fig. 12), the lowest WSS value (38.64 Pa) corresponded to a height of 0.220 m, while the highest WSS value (95.36 Pa) corresponded to a height of 0.190 m. Conversely, for the lowest height value (0.150 m), the WSS was 77.5 Pa and 64.2 Pa, while for the highest height value (0.300 m), the WSS was 60.02 Pa. The median was 60.80 Pa for a height of 0.200 m. Furthermore, for prostheses without endoleaks (Fig. 13), the lowest WSS value (42.76 Pa) corresponded to a height of 0.170 m, while the highest WSS value (104.79 Pa) corresponded to a height of 0.190 m. Conversely, for the lowest height value (0.150 m), the WSS was 87.13 Pa, while for the highest height value (0.300 m), the WSS was 67.44 Pa. The median was 68.31 Pa for a height of 0.200 m.

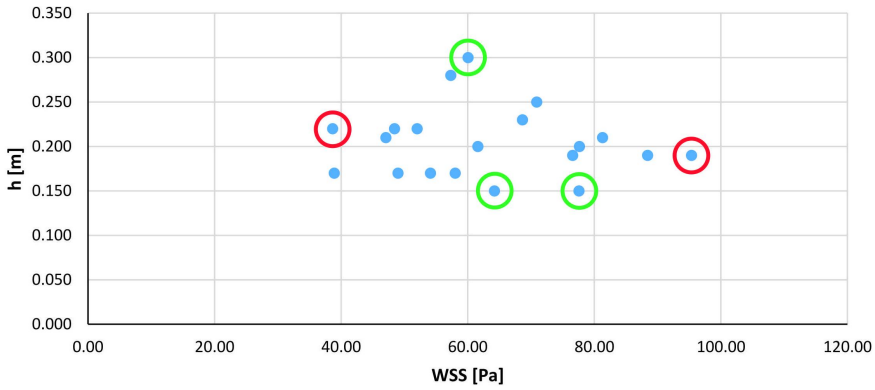

Fig. 12. Wall shear stress as a function of prosthesis height with an endoleak. Wall shear stress was measured in [Pa] and prosthesis height was measured in [m]. Red circles indicate exceptional points for WSS values and green circles indicate exceptional points for height values.

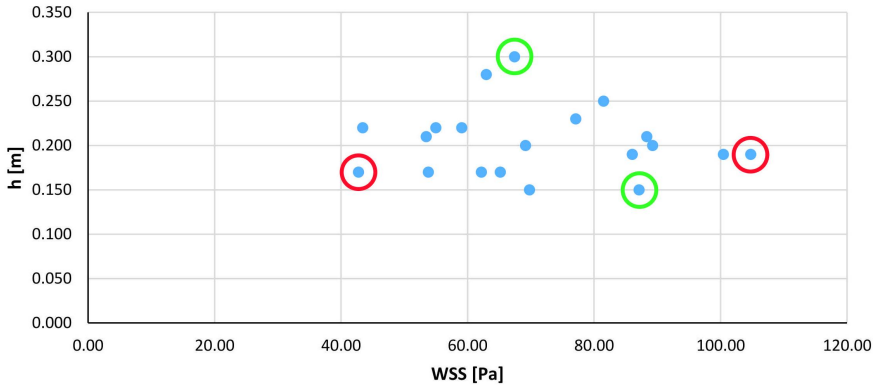

Fig. 13. Wall shear stress as a function of prosthesis height without an endoleak. Wall shear stress was measured in [Pa] and prosthesis height was measured in [m]. Red circles indicate exceptional points for WSS values and green circles indicate exceptional points for height values.

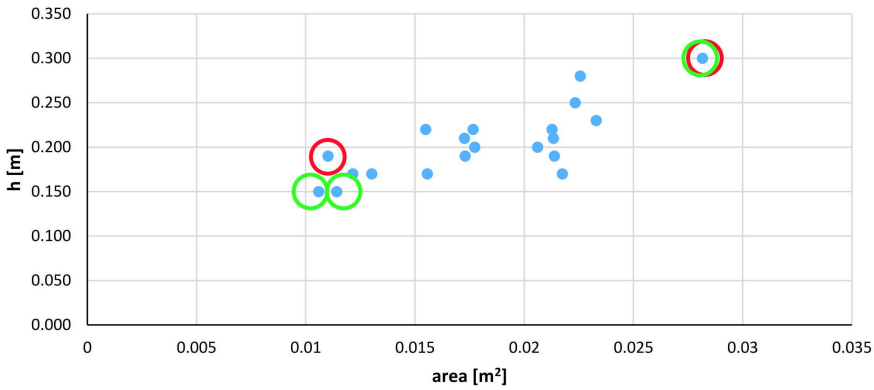

Fig. 14. Height as a function of prosthesis area with an endoleak. Height was measured in [m] and prosthesis area was measured in [m^2]. Red circles indicate exceptional points for height values and green circles indicate exceptional points for area values.

Moreover, a comparison of prosthesis height and area was analysed. It was observed that with an increase in the prosthesis area, there was an increase in height value. However, exceptions were observed: for prostheses with endoleaks (Fig. 14), the lowest area value (0.011 m^2) corresponded to a height of 0.190m, while the highest area value (0.280 m^2) corresponded to a height of 0.300 m. Conversely, for the lowest height value (0.150 m), the area was 0.011 m^2, while for the highest height value (0.300 m), the area was 0.280 m^2. The median was 0.180 m^2 for an area of 0.200 m^2. Furthermore, for prostheses without endoleaks (Fig. 15), the lowest area value (0.012 m^2) corresponded to heights of 0.150 m and 0.190 m, while the highest area value (0.031 m^2) corresponded to a height of 0.300 m. Conversely, for the lowest height value (0.150 m), the area was 0.012 m^2, while for the highest height value (0.300 m), the area was 0.031 m^2. The median was 0.020 m^2 for a height of 0.200 m.

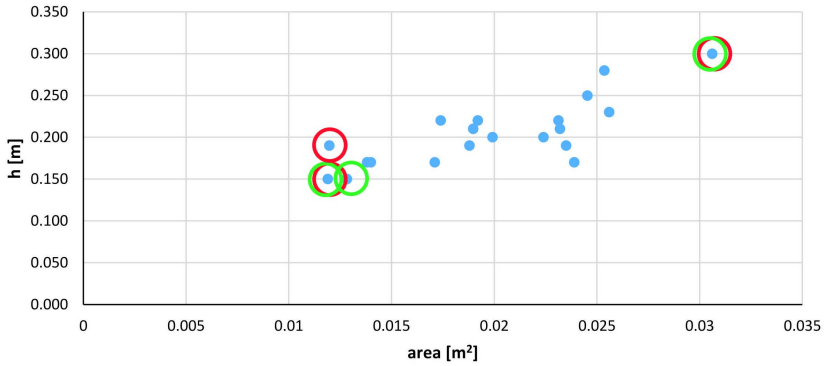

Fig. 15. Height as a function of prosthesis area without an endoleak. Height was measured in [m] and prosthesis area was measured in [m^2]. Red circles indicate exceptional points for height values and green circles indicate exceptional points for area values.

3.3. Shape factor

Finally, the influence of spatial configuration on the function of WSS was analysed. It was observed that for prostheses with endoleaks, the shape factor was equal to 1.23 ± 0.14, while for

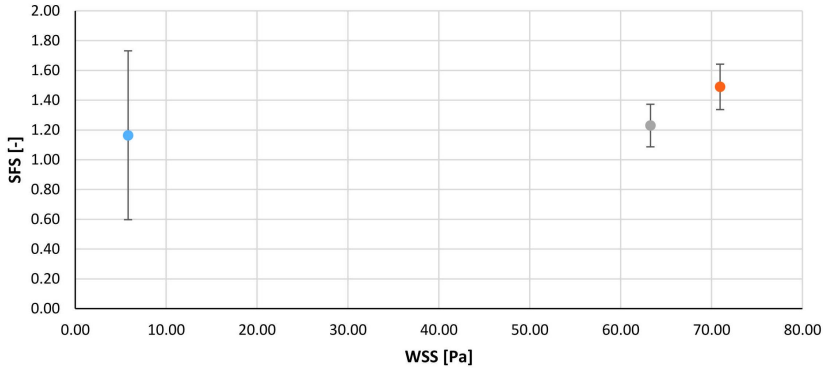

Fig. 16. Average shape factor as a function of prosthesis wall shear stress (blue colour), prosthesis with an endoleak (grey colour) and prostheses without an endoleak (orange colour). Wall shear stress was measured in [Pa].

the endoleak area, it was 1.16 ± 0.57, and for prostheses without endoleaks, it was 1.49 ± 0.15 (Fig. 16).

Analysis of prostheses with and without endoleaks indicated an increase in the WSS value with an increase in the shape factor. However, exceptions were observed: for prostheses with endoleaks (Fig. 17), the lowest WSS value (38.64 Pa) corresponded to a shape factor of 1.22, while the highest WSS value (95.36 Pa) corresponded to a shape factor of 1.12. Conversely, for the lowest shape factor value (0.96), the WSS was 47.05 Pa, while for the highest shape factor value (1.44), the WSS was 88.41 Pa. The median was 60.80 Pa for a shape factor of 1.26. Furthermore, for endoleaks (Fig. 18), the lowest WSS value (3.09 Pa) corresponded to a shape factor of 0.99, while the highest WSS value (7.63 Pa) corresponded to a shape factor of 0.70. Conversely, for the lowest shape factor value (0.43), the WSS was 4.06 Pa, while for the highest shape factor value (2.50), the WSS was 6.30 Pa. The median was 6.24 Pa for a shape factor of 0.97.

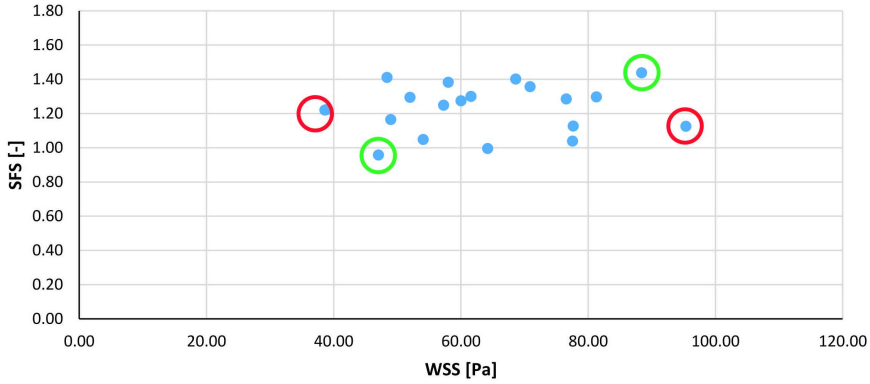

Fig. 17. Shape factor as a function of WSS for a prosthesis with an endoleak. Wall shear stress was measured in [Pa]. Red circles indicate exceptional points for WSS values and green circles indicate exceptional points for area values.

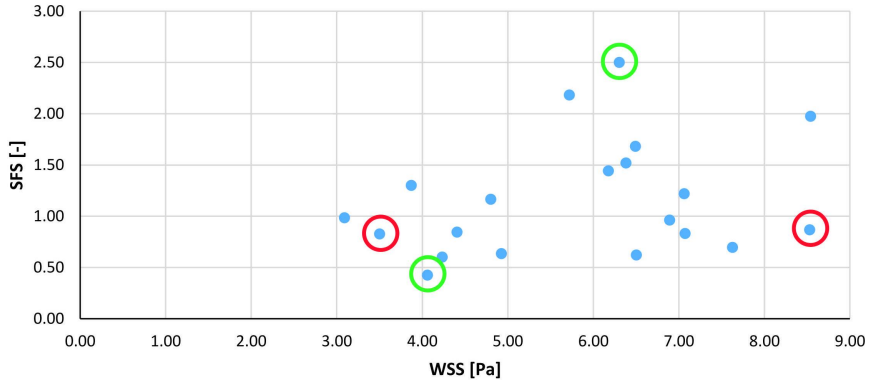

Fig. 18. Shape factor as a function of WSS for the endoleak area. Wall shear stress was measured in [Pa]. Red circles indicate exceptional points for WSS values and green circles indicate exceptional points for area values.

Moreover, analysis for prostheses without endoleaks (Fig. 19) indicated that for the lowest WSS value (42.76 Pa), the shape factor was 1.48, while for the highest WSS value (104.79 Pa), the shape factor was 1.33. Conversely, for the lowest shape factor value (1.16), the WSS was 53.47 Pa,

Metrol. Meas. Syst., Vol. 31 (2024), No. 4, pp. 711–731
DOI: 10.24425/mms.2024.152053

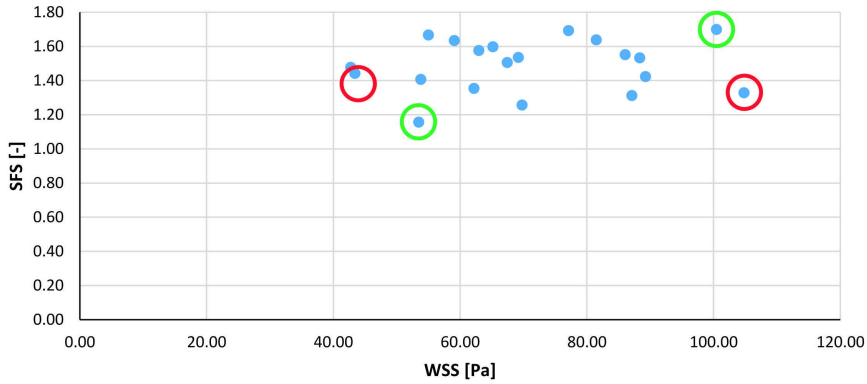

Fig. 19. Shape factor as a function of WSS for a prosthesis without endoleak. Wall shear stress was measured in [Pa]. Red circles indicate exceptional points for WSS values and green circles indicate exceptional points for area values.

while for the highest shape factor value (1.70), the WSS was 100.46 Pa. The median was 68.31 Pa for a shape factor of 1.52.

4. Discussion

The endovascular aneurysm repair procedure is performed to exclude the aneurysm sac from blood circulation. Therefore, the size of the abdominal aneurysm and the presence of endoleaks are crucial factors in evaluating the success of the treatment procedure [37]. This study presents a standardized process for analysing computer simulation results using shape factors related to spatial configuration and WSS values. The combination of computer simulations and medical imaging data is commonly employed for reconstructing hemodynamics in cardiovascular diseases [38]. In our previous research, we investigated the impact of stent-graft spatial configuration on the risk of leakage under realistic blood flow conditions [39]. In contrast to our approach, other studies often consider a perfectly tubular vessel with a straight axis and assume the stent-graft with less computational effort. However, this approach overlooks crucial elements such as the real angulation of the stent-graft directed by the shape of the aorta, as demonstrated in our work [40]. Literature analysis suggests that Type II endoleaks exert non-uniform pressure on the aneurysm sac [41]. Additionally, Nolz *et al.* observed that the presence of a Type II endoleak is associated with reduced movement of the surface in the proximal anchoring zone and the distal modular limb of bifurcated stent-grafts [42].

It was noted that therapeutic interventions could be enhanced with a deeper understanding of the mechanical behaviour of arteries [43]. A comparison of various stent-graft spatial configurations allowed for estimating the impact of changes in WSS in the region where endoleaks occur. It was observed that quantifying WSS in both normal and pathological arteries is a critical step [44]. Previous studies have demonstrated that alterations in blood hemodynamics affect the stable positioning of implants [45]. The analysis of wall shear stress on the 20 patient-specific models (before and after endoleak occurrence) indicated that higher WSS was observed in cases without endoleaks compared to those with endoleaks. Furthermore, higher WSS values were observed in the area of bifurcation as well as in the endoleak region. This finding is consistent with the observations of Szajer and Ho-Shon, who, using two methods (4D flow MRI and CFD techniques), observed similar phenomena, albeit in cases of aneurysms and carotid bifurcations [46]. The presented results suggest that the analysed topic is complex. They introduce a novel approach to

standardize the results of CFD algorithms based on the spatial configuration of stent-grafts. It has been demonstrated that merely considering the area and height of the stent-graft is insufficient for accurately describing WSS distribution. It is believed that in the future, analysing three-dimensional stent-grafts with varying degrees of tortuosity will be important.

The CFD algorithm facilitated the analysis of WSS values both before and after the occurrence of endoleaks, as well as within the endoleak region. A proposed shape factor characterized the spatial configuration of the stent-graft with and without endoleaks, accounting for the exerted pushing forces. It was noted that the algorithm generally indicated higher WSS values corresponding with higher shape factors, though there were exceptions. We believe that the presence of angular bends or tortuosity complicated the WSS estimation, suggesting this factor should be considered in future studies.

The proposed algorithm allows for assessing the risk level of postoperative complications associated with leaks in vascular prostheses. This solution also enables the digital fitting of the prosthesis before it is implanted in a specific Patient.

Limitations to the Study:

We acknowledge that the solution we have proposed has limitations. The relatively small sample size may affect the results obtained. However, the analysed groups were carefully selected for uniformity so that the results obtained may be applicable to other prostheses with endoleaks. Additionally, in the future, we intend to expand the sample size to assess the reliability of the CFD model. Furthermore, not all geometrical aspects were considered, such as tortuosity. Therefore, exceptions arose where an increase or decrease in the WSS value was not correlated with a higher or lower shape factor value.

Moreover, we utilized data with the highest possible resolution to minimize errors in three-dimensional reconstruction and the distribution of WSS results.

Acknowledgements

The study was approved by the local Institutional Review Board (2069/2012) of the Medical University of Vienna. The study was supported by the Polish National Centre for Research and Development (501/10-34-19-605 to AP) and by Grant number 181110 from the Medical University of Vienna, Department of Surgery, Division of Vascular Surgery (to IH). In the following study, the ANSYS Software affiliated to the BRaIn Laboratories of the Medical University of Lodz was used.

References

[1] Kwon, J., Dimuzio, P., Salvatore, D., & Abai, B. (2020). Incidence of stent graft failure from type IIIB endoleak in contemporary endovascular abdominal aortic aneurysm repair. *Journal of Vascular Surgery*, *71*(2), 645–653. https://doi.org/10.1016/j.jvs.2019.06.183

[2] Epple, J., Svidlova, Y., Schmitz-Rixen, T., Böckler, D., Lingwal, N., & Grundmann, R.T. (2023). Long-Term Outcome of Intact Abdominal Aortic Aneurysm after Endovascular or Open Repair. *Vascular and Endovascular Surgery*, *57*(8), 829–837. https://doi.org/10.1177/15385744231178130

[3] Yokoyama, Y., Kuno, T., & Takagi, H. (2020). Meta-analysis of phase-specific survival after elective endovascular versus surgical repair of abdominal aortic aneurysm from randomized controlled trials and propensity score-matched studies. *Journal of Vascular Surgery*, *72*(4), 1464–1472. https://doi.org/10.1016/j.jvs.2020.03.041

[4] Aggarwal, S., Qamar, A., Sharma, V., & Sharma, A. (2011). Abdominal aortic aneurysm: A comprehensive review. *Experimental & Clinical Cardiology*, *16*(1), 11–15.

[5] Knops, A.M., Ubbink, D.T., Legemate, D.A., de Haes, J.C.J.M., & Goossens, A. (2010). Information Communicated with patients in Decision Making about their Abdominal Aortic Aneurysm. *European Journal of Vascular and Endovascular Surgery*, *39*(6), 708–713. https://doi.org/10.1016/j.ejvs.2010.02.012

[6] Synowiec, T., Warot, M., Burchardt, P., & Chęciński, P. (2015). All dangerous types of endoleaks after endovascular aneurysm repair in a single patient. *Videosurgery and Other Miniinvasive Techniques*, 290–294. https://doi.org/10.5114/wiitm.2015.52600

[7] Rial, R., Serrano, F.J., Vega, M., Rodriguez, R., Martin, A., Mendez, J., Mendez, R., Santos, E., & Gallego, J. (2004). Treatment of Type II Endoleaks after Endovascular Repair of Abdominal Aortic Aneurysms: Translumbar Puncture and Injection of Thrombin into the Aneurysm Sac. *European Journal of Vascular and Endovascular Surgery*, *27*(3), 333–335. https://doi.org/10.1016/j.ejvs.2003.11.005

[8] Li, B., Khan, S., Salata, K., Hussain, M.A., de Mestral, C., Greco, E., Aljabri, B. A., Forbes, T. L., Verma, S., & Al-Omran, M. (2019). A systematic review and meta-analysis of the long-term outcomes of endovascular versus open repair of abdominal aortic aneurysm. *Journal of Vascular Surgery*, *70*(3), 954–969.e30. https://doi.org/10.1016/j.jvs.2019.01.076

[9] Cassagnes, L., Pérignon, R., Amokrane, F., Petermann, A., Bécaud, T., Saint-Lebes, B., Chabrot, P., Rousseau, H., & Boyer, L. (2016). Aortic stent-grafts: Endoleak surveillance. *Diagnostic and Interventional Imaging*, *97*(1), 19–27. https://doi.org/10.1016/j.diii.2014.12.014

[10] Nana, P., Dakis, K., Brodis, A., Spanos, K., Kouvelos, G., Eckstein, H.-H., & Giannoukas, A. (2022). A systematic review and meta-analysis on early mortality after abdominal aortic aneurysm repair in females in urgent and elective settings. *Journal of Vascular Surgery*, *75*(3), 1082–1088.e6. https://doi.org/10.1016/j.jvs.2021.10.040

[11] White, G.H., May, J., Waugh, R.C., Chaufour, X., & Yu, W. (1998). Type III and Type IV Endoleak: Toward a Complete Definition of Blood Flow in the Sac after Endoluminal AAA Repair. *Journal of Endovascular Therapy*, *5*(4), 305–309. https://doi.org/10.1177/152660289800500403

[12] Gil, F., Osowski, S., Świderski, B., & Słowińska, M. (2022). Ensemble of classifiers based on deep learning for medical image recognition. *Metrology and Measurement Systems*, *30*(1), 139–156. https://doi.org/10.24425/mms.2023.144400

[13] Roos, J.E., Hellinger, J.C., Hallet, R., Fleischmann, D., Zarins, C.K., & Rubin, G. D. (2005). Detection of endograft fractures with multidetector row computed tomography. *Journal of Vascular Surgery*, *42*(5), 1002–1006. https://doi.org/10.1016/j.jvs.2005.07.009

[14] Quaia, E. (2005). Detection of Endoleak After Endovascular Abdominal Aortic Aneurysm Repair. In: Quaia, E. (Eds.), *Contrast Media in Ultrasonography. Medical Radiology* (pp. 111–115). Springer. https://doi.org/10.1007/3-540-27214-3_9

[15] Suh, G.-Y., Les, A.S., Tenforde, A.S., Shadden, S.C., Spilker, R.L., Yeung, J.J., Cheng, C.P., Herfkens, R.J., Dalman, R.L., & Taylor, C.A. (2010). Quantification of particle Residence Time in Abdominal Aortic Aneurysms Using Magnetic Resonance Imaging and Computational Fluid Dynamics. *Annals of Biomedical Engineering*, *39*(2), 864–883. https://doi.org/10.1007/s10439-010-0202-4

[16] Polanczyk, A., Podyma, M., Trebinski, L., Chrzastek, J., Zbicinski, I., & Stefanczyk, L. (2016). A Novel Attempt to Standardize Results of CFD Simulations Basing on Spatial Configuration of Aortic Stent-Grafts. *PLOS ONE*, *11*(4), e0153332. https://doi.org/10.1371/journal.pone.0153332

[17] Chandrashekar, A., Handa, A., Lapolla, P., Shivakumar, N., Ngetich, E., Grau, V., & Regent Lee. (2020). Prediction of Abdominal Aortic Aneurysm Growth Using Geometric Assessment of Computerized Tomography Images Acquired During the Aneurysm Surveillance Period. *Annals of Surgery*, *277*(1), e175–e183. https://doi.org/10.1097/sla.0000000000004711

[18] Prucnal, M.A., & Polak, A.G. (2023). Single-channel EEG processing for sleep apnea detection and differentiation. *Metrology and Measurement Systems*, *30*(2), 323–336. https://doi.org/10.24425/mms.2023.144866

[19] Samartkit, P., & Pullteap, S. (2024). Non-Invasive Continuous Blood Pressure Sensors in Biomedical Engineering Research: A Review. *Sensors and Actuators A: Physical*, *367*, 115084. https://doi.org/10.1016/j.sna.2024.115084

[20] Ismail, S.N.A., Nayan, N.A., Jaafar, R., & May, Z. (2022). Recent Advances in Non-Invasive Blood Pressure Monitoring and Prediction Using a Machine Learning Approach. *Sensors*, *22*(16), 6195. https://doi.org/10.3390/s22166195

[21] Ismail, S.N.A., Nayan, N.A., Mohammad Haniff, M.A.S., Jaafar, R., & May, Z. (2023). Wearable Two-Dimensional Nanomaterial-Based Flexible Sensors for Blood Pressure Monitoring: A Review. *Nanomaterials*, *13*(5), 852. https://doi.org/10.3390/nano13050852

[22] Alter, P., Orszag, J., Wouters, E.F., Vogelmeier, C.F., & Jörres, R.A. (2022). Differences in the Measurement of Functional Residual Capacity Between Body Plethysmographs of Two Manufacturers. *International Journal of Chronic Obstructive Pulmonary Disease*, *Volume 17*, 1477–1482. https://doi.org/10.2147/copd.s363493

[23] Antonowicz, A., Wojtas, K., Makowski, Ł., Orciuch, W., & Kozłowski, M. (2023). Particle Image Velocimetry of 3D-Printed Anatomical Blood Vascular Models Affected by Atherosclerosis. *Materials*, *16*(3), 1055. https://doi.org/10.3390/ma16031055

[24] Lu, Y.-H., Mani, K., Panigrahi, B., Hsu, W.-T., & Chen, C.-Y. (2016). Endoleak Assessment Using Computational Fluid Dynamics and Image Processing Methods in Stented Abdominal Aortic Aneurysm Models. *Computational and Mathematical Methods in Medicine*, *2016*, 1–9. https://doi.org/10.1155/2016/9567294

[25] Bologna, E., Dinoto, E., Di Simone, F., Pecoraro, F., Ragusa, S., Siciliano, K., & Zingales, M. (2023). Computational Fluid Dynamics (CFD) and Finite Element Analysis (FEM) of a Customized Stent-Graft for Endovascular (EVAR) Treatment of Abdominal Aortic Aneurism (AAA). *Applied Sciences*, *13*(9), 5712. https://doi.org/10.3390/app13095712

[26] Materka, A., & Jurek, J. (2024). Using Deep Learning and B-Splines to Model Blood Vessel Lumen from 3D Images. *Sensors*, *24*(3), 846. https://doi.org/10.3390/s24030846

[27] Fung, G.S.K., Lam, S.K., Cheng, S.W.K., & Chow, K.W. (2008). On stent-graft models in thoracic aortic endovascular repair: A computational investigation of the hemodynamic factors. *Computers in Biology and Medicine*, *38*(4), 484–489. https://doi.org/10.1016/j.compbiomed.2008.01.012

[28] Peng, C., He, W., Huang, X., Ma, J., Yuan, T., Shi, Y., & Wang, S. (2023). The study on the impact of AAA wall motion on the hemodynamics based on 4D CT image data. *Frontiers in Bioengineering and Biotechnology*, *11*. https://doi.org/10.3389/fbioe.2023.1103905

[29] Polanczyk, A., Piechota-Polanczyk, A., Huk, I., Neumayer, C., Balcer, J., & Strzelecki, M. (2021). Computational Fluid Dynamic Technique for Assessment of How Changing Character of Blood Flow and Different Value of Hct Influence Blood Hemodynamic in Dissected Aorta. *Diagnostics*, *11*(10), 1866. https://doi.org/10.3390/diagnostics11101866

[30] Polanczyk, A., Piechota-Polanczyk, A., Stefańczyk, L., & Strzelecki, M. (2020). Spatial Configuration of Abdominal Aortic Aneurysm Analysis as a Useful Tool for the Estimation of Stent-Graft Migration. *Diagnostics*, *10*(10), 737. https://doi.org/10.3390/diagnostics10100737

[31] Polanczyk, A., Podgorski, M., Wozniak, T., Stefanczyk, L., & Strzelecki, M. (2018). Computational Fluid Dynamics as an Engineering Tool for the Reconstruction of Hemodynamics after Carotid Artery Stenosis Operation: A Case Study. *Medicina*, *54*(3), 42. https://doi.org/10.3390/medicina54030042

[32] Polanczyk, A., Piechota-Polańczyk, A., Stefanczyk, L., & Strzelecki, M. (2020). Shape and Enhancement Analysis as a Useful Tool for the Presentation of Blood Hemodynamic Properties in the Area of Aortic Dissection. *Journal of Clinical Medicine*, *9*(5), 1330. https://doi.org/10.3390/jcm9051330

[33] Polanczyk, A., Podgorski, M., Polanczyk, M., Veshkina, N., Zbicinski, I., Stefanczyk, L., & Neumayer, C. (2018). A novel method for describing biomechanical properties of the aortic wall based on the three-dimensional fluid-structure interaction model. *Interactive CardioVascular and Thoracic Surgery*, *28*(2), 306–315. https://doi.org/10.1093/icvts/ivy252

[34] Polanczyk, A., Piechota-Polanczyk, A., Neumayer, Ch., & Huk, I. (2019). CFD Reconstruction of Blood Hemodynamic Based on a Self-made Algorithm in patients with Acute Type IIIb Aortic Dissection Treated with TEVAR Procedure. In *IUTAM Bookseries* (pp. 75–84). Springer International Publishing. https://doi.org/10.1007/978-3-030-13720-5_7

[35] Polanczyk, A., Piechota-Polanczyk, A., Domenig, C., Nanobachvili, J., Huk, I., & Neumayer, C. (2018). Computational Fluid Dynamic Accuracy in Mimicking Changes in Blood Hemodynamics in patients with Acute Type IIIb Aortic Dissection Treated with TEVAR. *Applied Sciences*, *8*(8), 1309. https://doi.org/10.3390/app8081309

[36] Polanczyk, A., Podyma, M., Stefanczyk, L., Szubert, W., & Zbicinski, I. (2015). A 3D model of thrombus formation in a stent-graft after implantation in the abdominal aorta. *Journal of Biomechanics*, *48*(3), 425–431. https://doi.org/10.1016/j.jbiomech.2014.12.033

[37] Dias, N.V., Ivancev, K., Malina, M., Resch, T., Lindblad, B., & Sonesson, B. (2004). Intra-aneurysm sac pressure measurements after endovascular aneurysm repair: differences between shrinking, unchanged, and expanding aneurysms with and without endoleaks. *Journal of Vascular Surgery*, *39*(6), 1229–1235. https://doi.org/10.1016/j.jvs.2004.02.041

[38] Vergara, C., Le Van, D., Quadrio, M., Formaggia, L., & Domanin, M. (2017). Large eddy simulations of blood dynamics in abdominal aortic aneurysms. *Medical Engineering & Physics*, *47*, 38–46. https://doi.org/10.1016/j.medengphy.2017.06.030

[39] Polanczyk, A., Piechota-Polanczyk, A., Huk, I., Neumayer, C., & Strzelecki, M. (2022). Computational Fluid Dynamics as an Engineering Tool for the Reconstruction of Endovascular Prosthesis Endoleaks. *IEEE Access*, *10*, 18873–18885. https://doi.org/10.1109/access.2022.3150335

[40] Jayendiran, R., Nour, B., & Ruimi, A. (2018). Computational fluid–structure interaction analysis of blood flow on patient-specific reconstructed aortic anatomy and aneurysm treatment with Dacron graft. *Journal of Fluids and Structures*, *81*, 693–711. https://doi.org/10.1016/j.jfluidstructs.2018.06.008

[41] Dias, N.V., Ivancev, K., Resch, T.A., Malina, M., & Sonesson, B. (2007). Endoleaks after endovascular aneurysm repair lead to nonuniform intra-aneurysm sac pressure. *Journal of Vascular Surgery*, *46*(2), 197–203. https://doi.org/10.1016/j.jvs.2007.04.016

[42] Nolz, R., Schwartz, E., Langs, G., Loewe, C., Wibmer, A.G., Prusa, A.M., Teufelsbauer, H., & Schoder, M. (2015). Stent Graft Surface Movement after Infrarenal Abdominal Aortic Aneurysm

Repair: Comparison of patients with and without a Type 2 Endoleak. *European Journal of Vascular and Endovascular Surgery*, *50*(2), 181–188. https://doi.org/10.1016/j.ejvs.2015.03.031

[43] Susic, D., Varagic, J., Ahn, J., & Frohlich, E. (2004). Collagen Cross-link Breakers: A Beginning of a New Era in the Treatment of Cardiovascular Changes Associated with Aging, Diabetes, and Hypertension. *Current Drug Targets – Cardiovascular & Hematological Disorders*, *4*(1), 97–101. https://doi.org/10.2174/1568006043481347

[44] Chatzizisis, Y.S., Coskun, A.U., Jonas, M., Edelman, E.R., Feldman, C.L., & Stone, P.H. (2007). Role of Endothelial Shear Stress in the Natural History of Coronary Atherosclerosis and Vascular Remodeling. *Journal of the American College of Cardiology*, *49*(25), 2379–2393. https://doi.org/10.1016/j.jacc.2007.02.059

[45] Poon, E.K.W., Barlis, P., Moore, S., Pan, W.-H., Liu, Y., Ye, Y., Xue, Y., Zhu, S.J., & Ooi, A.S.H. (2014). Numerical investigations of the haemodynamic changes associated with stent malapposition in an idealised coronary artery. *Journal of Biomechanics*, *47*(12), 2843–2851. https://doi.org/10.1016/j.jbiomech.2014.07.030

[46] Szajer, J., & Ho-Shon, K. (2018). A comparison of 4D flow MRI-derived wall shear stress with computational fluid dynamics methods for intracranial aneurysms and carotid bifurcations — A review. *Magnetic Resonance Imaging*, *48*, 62–69. https://doi.org/10.1016/j.mri.2017.12.005

Professor **Andrzej Polańczyk** is a researcher at the Faculty of Safety Engineering and Civil Protection, Fire University, Warsaw. He earned ahis PhD in medical engineering in 2013. He Participated in scientific grants in which he built the installation to simulate the blood flow through the abdominal section of the aorta and computer algorithms for the 3D shape of aorta and blood hemodynamic reconstruction. His research areas comprise biomedical, chemical and, environmental engineering.

Professor **Aleksandra Piechota-Polańczyk** is currently employed at the Medical University of Lodz, Department of Cell Cultures and Genomic Analysis. Her research interests focus on finding new antioxidative and anti-inflammatory proteins that could be potential markers and/or targets in the treatment of cardiovascular and gastrointestinal diseases, as well as the role of Nrf2 and heme oxygenase 1 in cellular adaptation to oxidative stress and inflammatory reactions.

Professor **Agnieszka W. Piastowska-Ciesielska** is currently employed at the Medical University of Lodz, Department of Cell Cultures and Genomic Analysis. Her research interests focus on broadly understood xenobiotics that can modulate the functioning of both cancerous and normal cells. Her research focuses on assessing the impact of mycotoxins (produced by mould fungi) on cancer cells derived from the prostate gland.

Patricia Pia Wadowski - Professor Patricia Pia Wadowski is employed at the Department of Internal Medicine II, Division of Angiology at the Medical University of Vienna (Austria). Her research interests focus on microcirculation, peripheral arterial and aortic diseases, platelets and thromboinflammation.

Metrol. Meas. Syst., Vol. 31 (2024), No. 4, pp. 711–731
DOI: 10.24425/mms.2024.152053

Professor **Ihor Huk** has been the Director of the Vascular Laboratory and Clinical Professor of Surgery, Director of the Vascular Laboratory Department. of Surgery, MUV Medical School (Austria). He completed his post-graduate education at the University of Chicago, Heidelberg Special Training: American Society in Parenteral and Enteral Nutrition. Transplant surgery: Since 1984 he has performed more than 550 kidney and liver transplantations. Vascular Surgery: Clinical, experimental Research (SPACE-Study), (L-arginine study). He is a member of the Austrian Society of Surgery, Austrian Society of Angiology, Austrian Society of Vascular Surgery, Ukrainian Academy of High Education, Ukrainian Academy of Sciences and Senate -Zaporizhzhia Medical Postgraduate Academy Honoris causa.

Professor **Christoph Neumayer** is the Head of the Department of Vascular Surgery at the Medical University of Vienna. His main research area is the molecular mechanism of artery diseases and diabetes.

Julia Balcer is currently a student at Lodz University of Technology, Poland. Her research interests focus on processing and analysis of images and data analysis methods.

Professor **Michal Strzelecki** is employed at the Institute of Electronics, Lodz University of Technology, Poland. His scientific interests include the processing and analysis of biomedical signals and images, data analysis methods, and artificial intelligence. He also works on the development of software aimed at supporting medical imaging diagnostics. Within his area interest, Prof. Strzelecki has conducted extensive cooperation with domestic and foreign medical universities on the construction and development of systems supporting the diagnostic process.